Multimedia Tools and Applications (2020) 79:17169–17192
https://doi.org/10.1007/s11042-019-07762-3

Active contour with modified Otsu method for automatic detection of polycystic ovary syndrome from ultrasound image of ovary

C. Gopalakrishnan [1] · M. Iyapparaja [1]

Received: 6 February 2019 / Revised: 16 April 2019 / Accepted: 9 May 2019 /
Published online: 8 November 2019

Abstract
Polycystic ovary syndrome (PCOS) disorder is identified by the presence of a number of follicles present in the ovary of female reproductive system. Ultrasound imaging of the ovary contains essential information about the size, number of follicles and its position. In real time, the detection of PCOS is a difficult task for radiologists due to the various sizes of follicles and is highly connected with blood vessels and tissues. This often results in error diagnosis. For preprocessing various standard filtering techniques are applied on ovary image. Based on the performance, appropriate filter is chosen to remove the noise from the image. This paper presents an effectual active contour with modified Otsu threshold value to automated discovery of follicles from the ultrasound images. The performances of the proposed method illustrate the betterments of the proposed approach over other techniques.

Keywords Follicle · PCOS · Ultrasound image active contour · Modified Otsu

1 Introduction

Polycystic ovary syndrome prevails as a complex endocrine disorder causing adverse effects in women's health. Presence of follicular cysts in an ovary of female reproductive system is the characterization of this disorder. PCOS obstruct the balance of follicle stimulating hormone and luteinizing hormone which needs for an egg to mature properly inside the ovaries [31]. The accumulation of incompletely developed follicles leads to PCOS which have the common symptoms of infertility, irregularity in menstrual cycles to stoppage of menstrual period, unwanted hair growth on the face and body, unusual weight gain, getting obese, acne and

✉ C. Gopalakrishnan
arungopalit@gmail.com

M. Iyapparaja
Iyapparaja@vit.ac.in

[1] School of Information Technology and Engineering, VIT University, Vellore, India

hyperinsulinemia [2–5, 15, 20, 30, 31, 35]. Medical imaging techniques such as CT, MRI and Ultrasound techniques are accustomed to viewing the human body in order to identify the symptoms, derive a treatment plan and monitor the progress of medications. Ultrasound is mainly used for imaging liver, kidney, uterus because of its noninvasive nature also it is portable, transferable, adaptable, have excellent temporal resolution, and they are relatively inexpensive. These should leads to an ultrasound assessment of ovaries. These evaluations give immense insight into the condition of the ovary and number of follicle presents in it. As a result of poor quality of ultrasound images the misinterpretation of pcos is possible. Number of follicles is not specific for the polycystic ovaries, sometimes the normal ovary also contains more number of follicles [20]. To differentiate polycystic ovary from multiple follicles of normal ovary, a standard criteria has been put forth by EuropeanSociety of Human Reproduction and Embryology, the American Society for Reproductive.

Otsu Concept: It performs image thresholding automatically which is based on clustering method or in other terms it reduces the graylevel-image to binary-image. It assumes two classes of pixels is contained in the image followed by the bi-modal histogram and optimum threshold is calculated by separating the two-classes in which combined spread should be minimal. Follicle Count: It is the study of transvaginal ultrasound for measuring the reserved women's ovarian which is small and fluid filled sac containing the immature egg.

According to previous understanding from medical industries, polycystic ovaries are said to have more than 12 follicles with 2 – 9 mm in diameter. During image acquisition phase, noise is introduced in the acquired image in a lot of possible way. The air gap between human body and the transducer probe introduces the noise in the image which will affect the diagnosis [5]. When compare to CT and MRI modalities ultrasound image contains excess of noise particularly Speckle Noise. Speckle noise is multiplicative in nature which will make diagnosis difficult, by degrades edge and smallest discernible detail in an image. The resolution and the quality of an image are highly based on the frequency range and the transducers used in the probe. Nowadays at the time of acquisition to improve the quality of an ultrasound images higher end ultrasound machines are introduced with high quality transducers in the probe, also the gel is used to reduce the air gab between the probe and the human body. After acquisition, to improve the segmentation result and for accurate diagnosis, ultrasound ovary images are filtered using various image denoising techniques. To exactly discover the number of follicles in the ultrasound ovary image, it is necessary to reduce the speckle noise. From the list of filtering techniques available today, many are powerful enough to include a diverse range of parameters to be controlled and adjusted to retrieve better performance. The radiologist using conventional ultrasound machine to scan the ovary and they are rotates the probe progressively to scan ovaries although first recognize each follicle and then measuring its size and dimension. This system is manual, time-consuming also painful to the patient. To overcome these automated method is introduced for the detection and counting of follicles.

In literature, several contributions on noise reduction using novel methods implementing thresholds for wavelets to reduce the effects of speckle noise were introduced. The threshold values are obtained from assigning weights to variance levels. It is observed that sharpness of images are disturbed by the effects of applied filters whereas a wavelet threshold is not affecting the sharpness by any means [34]. This is because of the fact that wavelet transform produces better results when compared to the median and wiener filter [27]. A modified morphological image cleaning algorithm is introduced which is implemented by a mathematical morphology operation based on set theory. The disadvantage in this algorithm is that the morphological filter tends to lose the features with respect to varying size of structuring

elements [33]. Michailovich et al. introduces a despeckling method for ultrasound images, these method without disturbing the medical image anatomical content remove the noise from the image [24].

Due to the insufficiency of hormones the egg does not mature properly and results in failure of ovum release. In medical diagnosis, identifying follicles from ultrasound image is a critical issue. Modified watershed algorithms are used to extract follicles from ovary which results in over segmentation. The output of the watershed algorithm is given as an input to the clustering algorithm produces better recognition rate [9]. Edge based segmentation method results in broken edges. Morphological operations are used to overcome these problems. Shrinkage of images may lose vital details from an image. For medical imaging, accurate results are needed for effective diagnosis [17]. To efficiently segment follicles region growing methods were introduced. These methods initially require an expert's intervention in choosing a seed point which also comes under manual detection of follicles. Region growing methods will be minimally affected by to noise and increase the chances of recognition [10]. Morphological operators often take a binary image followed by opening and closing operations were used to derive the bright features from the ultrasound images' background by using Tophat transform. Scanline segmentation then acts upon the enhanced images for a lesser error rate than manual detection [23].

The contrast of a de-speckled image is improved by using Histogram Equalization. The proposed method is designed to work on objects possessing high intensity values and thus the negative transformation is applied to the histogram equalized. During the segmentation phease, edges removed active contour is used. After this application of active contour method, the resultant image will contain segmented regions [16]. Thresholding is the easiest and effective methods to achieve optimal threshold value to binarize the grayscale image. Otsu method is a global threshold selection method widely used because of its simplicity and quality [6–8, 18, 19, 25, 26, 28, 29, 32]. The problems related to energy minimization approach were solved by new active contour model following the level set framework. During the curve evolution the changes in the contour solved implicitly are highlighted advantage of the level set method [32]. In medical imaging to segment region of interest level set methods are used. Chan and Vese introduces active contours method also consider information inside the region they solve this problem using level set methods [7], the geometric active contour models are proposed by Caselles et al. these methods based on speed term [6]. Mohammed Ammar et al. introduced thresholding to initialize the level set segmentation. The binary mask is obtained from thresholding [19]. Senthil Murugan N and Usha Devi G proposed a hybrid extraction and classification model for tweet data which is major research over hybridization of algorithms to analyze the large source easily [1, 13, 25, 26].

The following sections are organized as follows. The flow of the paper is explained in section II. The denoising filtering techniques and its performance are explained in Section III. In Section IV Otsu's method is described briefly and proposed method is introduced. Section V discuss about the feature extraction. Results obtained from different methods are provided in Section VI, and conclusions are drawn in Section VII.

2 Methods

The input to the automatic detection of PCOS system is the ultrasound image of ovary. The ovary occupies only a small region in the entire ultrasound image, Region of Interest (ROI) is

extracted from the input image. The ultrasound images are attributed to speckle noise, so in pre-processing stage speckle noise is removed using various speckle filtering techniques. Scalar technique: Scalar channels depend on the proportion of nearby measurements, which improves smoothing in homogenous areas of the pictures where spot is completely created and diminishes obviously in different locales of the picture so as to safeguard the valuable subtleties of the picture. Key sorts of scalar channels are Mean channel and Median channels talked about in next segments. A ROI extraction is used to filter a portion of an image for the filter operations. It is abbreviated as region of interest (ROI). In the follicle identification phase the follicles are segmented using proposed method and the features such as area, major axis, minor axis, and eccentricity are extracted from the segmented results. Based on the feature information the ovary is classified as normal/ abnormal. The block diagram of the proposed method is shown in Fig. 1.

3 Speckle noise reduction in ultrasound images

An automatic segmentation of ultrasound medical images produces less accurate result due to speckle noise known as multiplicative noise. Medical ultrasound imaging, uses sound waves and their echoes to scan the human body, due to the interference of echoes produced by reflectors introduces speckle noise in the image, which degrades the quality of an image. The recent version of the ultrasound systems like GE LOGIQ and Siemens, exclusively deliver various image denoising techniques to remove speckle noise in the image. The images obtained from these systems gives noise free image. In this paper, for pre-processing of an image various filtering techniques are applied on ultrasound ovary image. The performances of filtering techniques are evaluated using different metrics and the results are tabulated.

The mathematical expression of multiplicative noise model is given by

$$\overline{k}[a,b] = k[a,b] + \eta[a,b]k[a,b] \tag{1}$$

Let k [a,b] be the original ultrasound ovary image. $\overline{k}$[a, b]be the digitized version of noise and η[a,b] is the noise function [14].

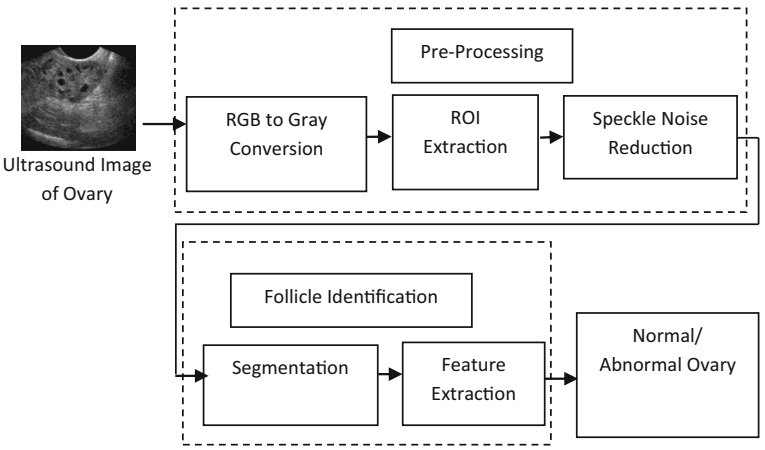

Fig. 1 Block diagram of automatic detection of ovarian follicles

3.1 Lee filter

Lee filter is a statistical filter based on Minimum Mean Square Error criterion [22]. Lee filter with window size of 3 × 3, 5 × 5, 7 × 7 are used to reduce speckle noise. The main drawback of lee filter is that it failure to remove noise in the edges and lines.

The formula for Lee filter is given as

$$\hat{K}(r,s) = g(r,s)w(r,s) + \overline{g(r,s)}(1-w(r,s)) \tag{2}$$

Where *w(r,s)* is the weighted function.

$$w(r,s) = 1-{c_x^2}\Big/{c_g^2(r,s)} \tag{3}$$

3.2 Kuan filter

Kuan filters are used to reduce speckle noise from the medical ultrasound images in order to preserve edges in an image. The Kuan filter is same as the lee filter but it uses the different weighting function [21].

$$w(r,s) = \frac{1-{c_x^2}\Big/{c_g^2(r,s)}}{1+c_x^2} \tag{4}$$

3.3 Frost filter

The filter approximates the noise-free image by convolving the observed image with a spatially-varying kernel [12] as.

$\overline{K}(r,s) = g(r,s)*m(r,s)$. The kernel *m(r, s)* centered at the pixel location (x_0, y_0), is given as

$$m(r,s) = D_1 \exp\left(-DC_1^2(r_0,s_0)|r,s|\right) \tag{5}$$

Where the parameter D is used for controlling the dampening rate, $|r,s|$ is used to denote the distance of each pixel from (r_0,s_0), and D_1 is a constant used for normalizing. An estimate for C_n is not required in this approach[11]. Parameter D must be chosen based on homogeneous regions with inhibited edges after mean filtering process is implemented. When compared to Lee and Kuan filter, Frost filter produces better results for ultrasound ovary images. The performance of the filter is evaluated using the estimation parameters.

3.4 Median filter

The Median filter is non linear in nature, that first sort all the specific neighborhood pixel values in the original image based on the size of their intensity values and replaces the median pixel value in the window by center pixel value of its neighbors [14]. For certain types of random noise median filter provides excellent noise reduction capabilities and it preserves edges. In this paper median filter with window size of 3 × 3, 5 × 5 and 7 × 7 applied on the ovary image. The experimental result shows that the filter with smaller window size yields better quality image.

3.5 Gaussian filter

The Gaussian low pass filter removes the noise as a result of blurring images. Gaussian kernel uses a different kernel. The Gaussian filter has the more familiar form [14]

$$g(r,s) = e^{-C_f{}^2(r,s)/2C_{f_o}^2} \tag{6}$$

where $C_{f(r,s)}$ is the distance from the origin of the Fourier transform and C_{f_0} is the cut off frequency.

3.6 Wiener filter

The wiener filter, a data- dependent linear filter is the most important technique used to suppress the noise added in the signal. For instance images degraded by blurring and additive noise due to linear motion or unfocussed optics. MSE-optimal stationary linear filter is used in wide range of applications such as echo cancellation, channel equalization, signal restoration and linear prediction. The wiener filter is used to restore the image which is based on the local image variance [14]. The Wiener filter equation is given by

$$I(x,y) = \left[\frac{H^{'}(x,y)}{H(x,y)^2 + \left[\frac{K_n(x,y)}{K_f(x,y)}\right]}\right] F(x,y) \tag{7}$$

where H(x,y) is the degradation function and H′(x,y) is the conjugate complex.

3.7 Performance evaluation

The quality of an image is important when processing medical ultrasound images. The visual perception is improved in the denoised images which makes the diagnosis easier. The evaluation metrics like Mean Square Error (MSE), Peak Signal to Noise Ratio (PSNR), Normalized Cross Correlation (NK), Absolute Difference (AD), Structural Content (SC), Maximum Difference (MD). Normalized Absolute errors (NAE) are illustrated below. These metrics are calculated using original image g and the filtered image $g^{'}$.

3.7.1 Mean square error (MSE)

The MSE measures the total amount of difference between the original image and filtered image.

$$MSE = \frac{1}{RC}\sum_{s=1}^{R}\sum_{k=1}^{C}\left(G(s,k) - G^{'}(s,k)^2\right. \tag{8}$$

3.7.2 Peak signal to noise ratio (PSNR)

It is an evaluation parameter to evaluate the performance of the filters. The PSNR is higher for the good quality image and it is lower for the poor quality image.

$$PSNR = 10\log\frac{255^2}{MSE} \tag{9}$$

3.7.3 Normalized cross correlation (NK)

The normalized cross correlation measure is described as

$$NK = \sum_{s=1}^{R}\sum_{k=1}^{C} G(s,k).G^{'}(s,k) / \sum_{s=1}^{R}\sum_{k=1}^{C} G^2(s,k) \tag{10}$$

3.7.4 Absolute difference (AD)

The absolute difference is described as

$$AD = \sum_{s=1}^{R}\sum_{k=1}^{C} \left(G(s,k) - G^{'}(s,k)\right)/RC \tag{11}$$

In Eq. 11.G and $G^{'}$ are the original image and denoised image. R and C are the rows and columns of an image.

3.7.5 Structural content (SC)

The structural content of an image is given in the Eq. 12.

$$SC = \sum_{s=1}^{R}\sum_{k=1}^{C} G^2(s,k) / \sum_{s=1}^{R}\sum_{k=1}^{C} G^{'2}(s,k) \tag{12}$$

The smallest value of structural content shows better quality of an image whereas highest value of structural content is evidence for poor quality image.

3.7.6 Maximum difference (MD)

The maximum difference of an image is described as

$$MD = Max\left(\left|G(s,k) - G^{'}(s,k)\right|\right) \tag{13}$$

The smallest value of maximum difference means the image is better quality.

3.7.7 Normalized absolute error (NAE)

The normalized absolute error of filtered image is defined as

$$NAE = \sum_{s=1}^{R}\sum_{k=1}^{C} \left|G(s,k) - G^{'}(s,k)\right| / \sum_{s=1}^{R}\sum_{k=1}^{C} \left|G(s,k)\right| \tag{14}$$

The largest value of normalized absolute error shows the image is poor quality.

The Lee filter, Kuan filter, Frost filter, Median filter and Wiener filter are implemented using kernel size of 3×3, 5×5, 7×7, the Gaussian low pass filter are implemented using different cut off frequency 10, 20 and 30The Fig. 2(a) shows an original ultrasound ovary

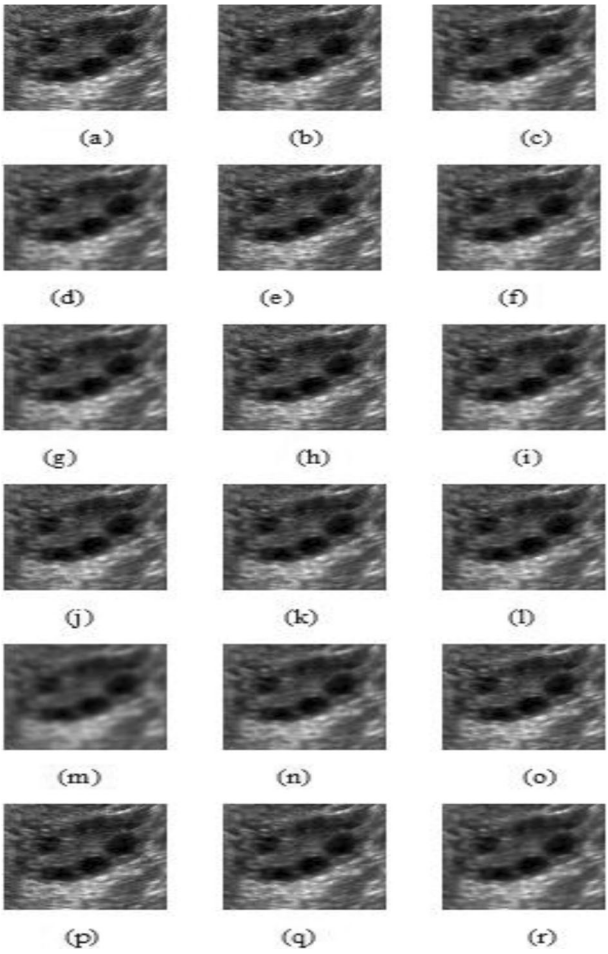

Fig. 2 (a) Original Image (b) Frost 3 × 3 (c) Frost 5 × 5 (d) Frost 7 × 7 (e) Lee 3 × 3 (f) Lee 5 × 5 (g) Lee 7 × 7 (h) Kuan 3 × 3 (i) Kuan 5 × 5 (j) Median 3 × 3 (k) Median 5 × 5 (l) Median 7 × 7 (m) Gaussian $f_c = 10$ (n) Gaussian $f_c = 20$ (o) Gaussian $f_c = 30$ (p) Wiener 3 × 3 (q) Wiener 5 × 5 (r) Wiener 7 × 7

image and the resultant images of different denoising filters are shown in Fig. 2 (b)–(r). For evaluating the performance of denoising filter various metrics are measured Mean Square Error (MSE), Peak Signal to Noise Ratio (PSNR), Normalized cross correlation (NK), Absolute Difference (AD), Structural Content (SC), Maximum Difference (MD), Normalized Absolute Error (NAE). For the Figs. 3-9 denoising filters are taken on x-axis and performance metrics is taken on y-axis which depicts the performance of the filter.

Tables 1, 2 and 3 provides additional results to observe the filter performance in terms of MSE, PSNR, NK, AD, SC, and MD for Test Image 1, Test Image 2 and Test Image 3 respectively. Minimizing the MSE, NAE, NK, SC, AD and maximizing the PSNR values results in a filter which is the best among the other denoising filter. From the Figs. 3, 4, 5, 6, 7, 8 and 9, we examined that the Frost filter with kernel size 3 × 3 gives better results than other denoising filters. The Median and Wiener filters are mainly used to remove additive noise. Median filter works well for salt & pepper noise, whereas it produces poor results for

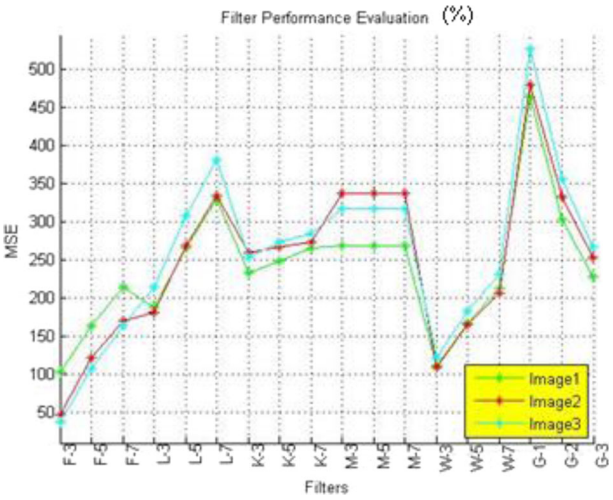

Fig. 3 MSE-Filter performance graph

denoising multiplicative noise. Gaussian low pass filter produces better result for denoising speckle from image but which results in more blurred images fine details are loosed in this process. Lee, Kuan, Frost, Median, Wiener and Gaussian filters are applied on 65 ultrasound ovary images and the performances are evaluated. The results are tabulated and each metrics values for different filters are plotted separately. In this paper the experimental results of three ultrasound image is shown to ensure the consistency of results.

In this paper the experimental results of three ultrasound image is shown to ensure the consistency of results. From the performance metrics Tables 1, 2, 3, and from the plots it is observed that Frost filter with kernel size 3 × 3 is better among all the other filters for denosing ultrasound ovary images.

As discussed previous, nowadays most ultrasound systems itself contains despeckling filters, for this work the testing images are acquired using latest GE system. Even though at

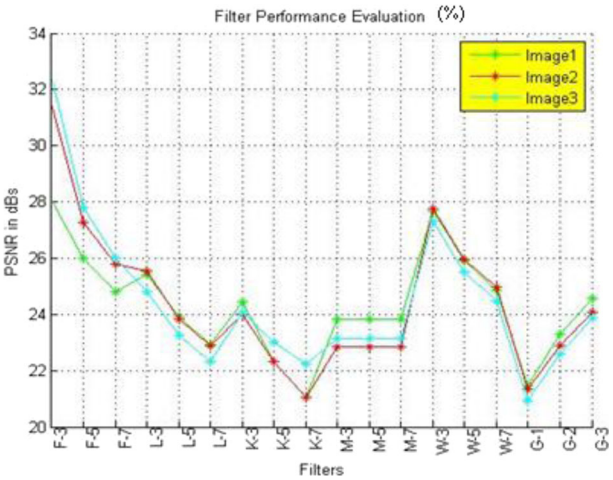

Fig. 4 PSNR-Filter performance graph

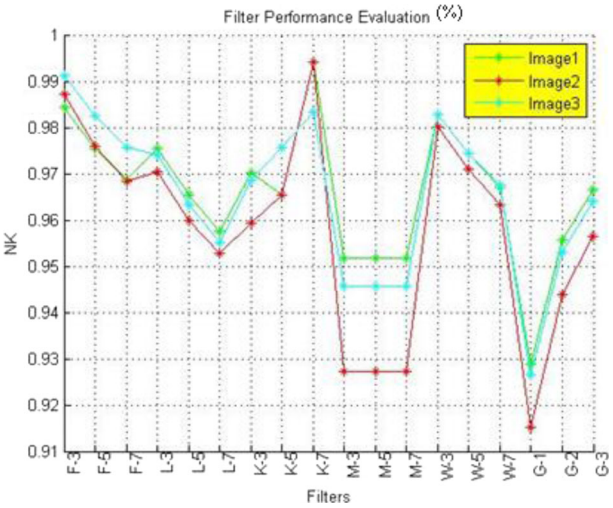

Fig. 5 NK-Filter performance graph

the time of transmission there is chance for contamination, for furthering processing the images are preprocessed using standard filter.

The ultrasound images are denoised by various filters which are shown in the Fig. 2. for visual assessment. The Fig. 2 shows all methods achieve better speckle suppression. Gaussian methods blur the image to remove noise, but it is not suitable for accurate diagnosis of medical images. Wiener filter successfully denoised the image with the kernel size of 3×3. Several important details have lost by Lee and Kuan filters in which the result of the images at the end is blurred. In addition, better visual enhancement is yielded by Frost filter having the kernel size of 3×3 for ultrasound ovary images. The optimum value is obtained from Frost filter which satisfies four metrics. For Frost Filter peak signal to ratio is high and mean square error, normalized absolute error and structural content is low. The main disadvantage of Lee filter

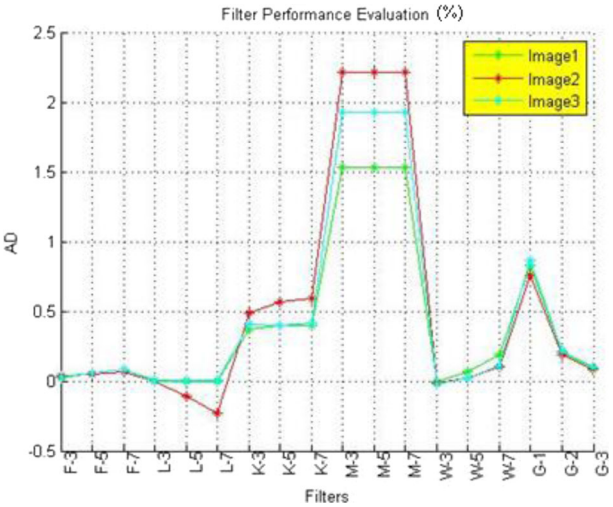

Fig. 6 AD-Filter performance graph

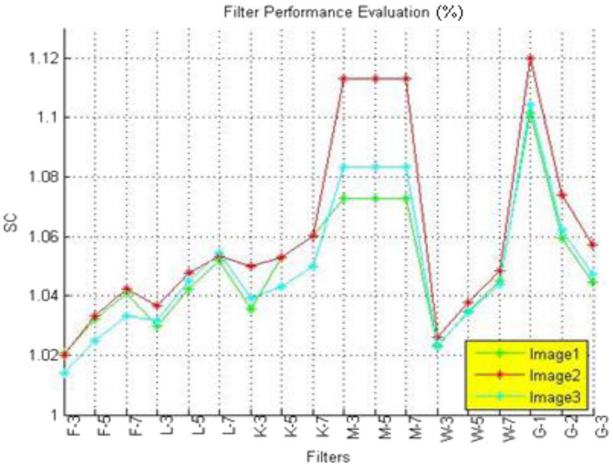

Fig. 7 SC-Filter performance graph

over other filtering techniques is that it fails to remove speckle noise in the region near to the edges. The performance of the Frost filter is better than the other filters.. Based on the performance metrics the filter is chosen to preprocess the ultrasound image. The denoised image is used for further processing.

4 Follicle segmentation

Segmentation is defined as the process of partitioning an image into meaningful sub region that exhibit desired features. Segmenting follicles from ovary image is a difficult task due to the presence of soft tissue, ordinary tissue and blood vessels. Thresholding is an effective technique to discriminating objects from background which is based on the principle of minimization function produces an optimal threshold value. The choice of threshold must be made empirical by considering the nature of their image and the number of objects expected

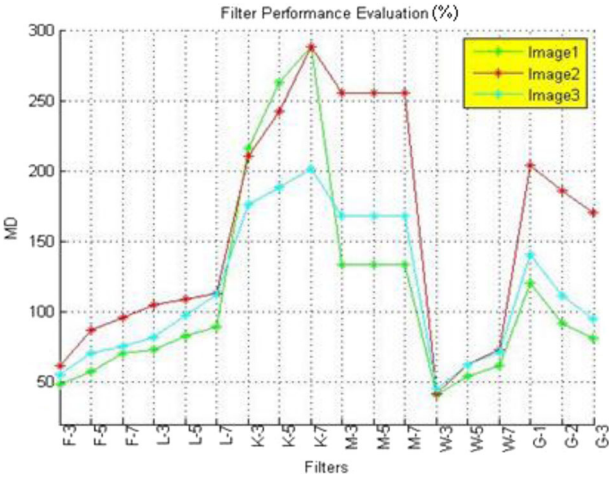

Fig. 8 MD-Filter performance graph

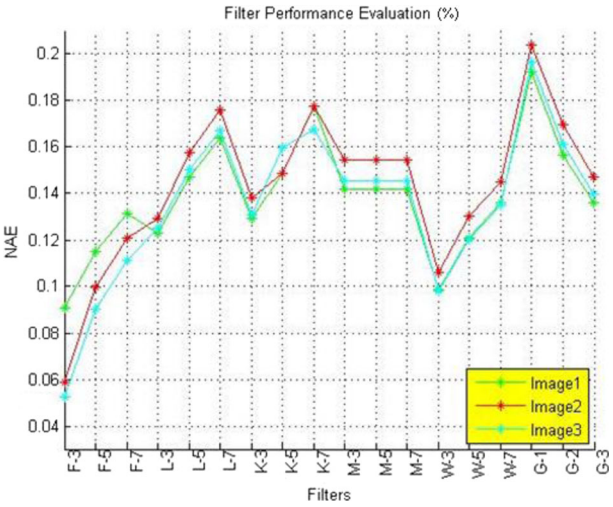

Fig. 9 NAE-Filter performance graph

from the image. The Otsu method binarizes the image into two groups based on the principle of minimization of within class variance. In this section we review the Otsu and Proposed method for accurate segmentation of follicles from the ovary image.

4.1 Otsu method

Otsu's method [29] finds the optimal threshold, from the histogram of an image to binarize the image into two groups. The means of the two groups are computed as μ_1 and μ_2.

Table 1 Performance metrics of different denoising filters for test image 1

Filters	Window Size /Frequency	Performance Metrics						
		AD	MD	MSE	NAE	NK	PSNR	SC
Frost	3 × 3	0.0212	48.0000	**102.4883**	**0.0907**	0.9843	**28.0240**	**1.0206**
Frost	5 × 5	0.0562	57.0000	163.7236	0.1150	0.9754	25.9896	1.0322
Frost	7 × 7	0.0859	70.0000	214.1449	0.1313	0.9687	24.8237	1.0408
Lee	3 × 3	0.0013	73.0000	187.2249	0.1229	0.9754	25.4071	1.0296
Lee	5 × 5	−0.0028	83.0000	265.1261	0.1472	0.9653	23.8962	1.0423
Lee	7 × 7	−0.0012	89.0000	330.6231	0.1641	0.9574	22.9374	1.0520
Kuan	3 × 3	0.3739	216.0000	233.0798	0.1291	0.9701	24.4557	1.0357
Kuan	5 × 5	0.3980	263.000	248.0230	0.1488	0.9653	22.3082	1.0532
Kuan	7 × 7	0.4012	288.000	266.0564	0.1775	0.9940	21.0378	1.0603
Median	3 × 3	1.5291	133.0000	268.2068	0.1415	0.9516	23.8461	1.0726
Median	5 × 5	1.5214	133.0000	268.2068	0.1415	0.9516	23.8461	1.0726
Median	7 × 7	1.5291	133.0000	268.2068	0.1415	0.9516	23.8461	1.0726
Wiener	3 × 3	**−0.0059**	**41.0000**	111.1159	0.0984	0.9828	27.6730	1.0229
Wiener	5 × 5	0.0657	54.0000	166.9460	0.1208	0.9742	25.9050	1.0346
Wiener	7 × 7	0.1869	61.0000	212.6449	0.1359	0.9669	24.8542	1.0450
Gaussian	($f_c = 10$)	0.8274	120.0000	464.2543	0.1923	**0.9289**	21.4632	1.1016
Gaussian	($f_c = 20$)	0.2086	92.0000	303.9156	0.1568	0.9556	23.3032	1.0593
Gaussian	($f_c = 30$)	0.0928	81.0000	228.2826	0.1362	0.9664	24.5460	1.0445
Optimum Value		**−0.0059**	**41.0000**	**102.4883**	**0.0907**	**0.9289**	**28.0240**	**1.0206**

Table 2 Performance metrics of different denoising filters for test image 2

Filters	Window Size/Frequency	Performance Metrics						
		AD	MD	MSE	NAE	NK	PSNR	SC
Frost	3 × 3	0.0366	61.0000	**46.3289**	**0.0588**	0.9871	**31.4722**	1.**0198**
Frost	5 × 5	0.0494	87.0000	121.8180	0.0997	0.9758	27.2736	1.0332
Frost	7 × 7	0.0696	96.0000	170.8821	0.1208	0.9683	25.8038	1.0424
Lee	3 × 3	−0.0011	105.0000	180.8032	0.1290	0.9704	25.5587	1.0368
Lee	5 × 5	−0.1068	109.0000	268.6752	0.1576	0.9598	23.8385	1.0475
Lee	7 × 7	**−0.2327**	113.0000	335.3208	0.1759	0.9528	22.8762	1.0533
Kuan	3 × 3	0.4884	210.0000	259.9604	0.1383	0.9593	23.9817	1.0500
Kuan	5 × 5	0.5693	242.000	267.0230	0.1488	0.9653	22.3082	1.0532
Kuan	7 × 7	0.5892	288.000	274.0364	0.1775	0.9940	21.0378	1.0603
Median	3 × 3	2.2129	255.0000	338.4599	0.1544	0.9271	22.8357	1.1130
Median	5 × 5	2.2129	255.0000	338.4599	0.1544	0.9271	22.8357	1.1130
Median	7 × 7	2.2129	255.0000	338.4599	0.1544	0.9271	22.8357	1.1130
Wiener	3 × 3	−0.0099	**42.0000**	109.4000	0.1061	0.9802	27.7406	1.0259
Wiener	5 × 5	0.0231	62.0000	165.5110	0.1302	0.9709	25.9425	1.0378
Wiener	7 × 7	0.1024	73.0000	206.7101	0.1451	0.9634	24.9771	1.0484
Gaussian	($f_c = 10$)	0.7570	204.0000	480.5405	0.2042	**0.9152**	21.3135	1.1197
Gaussian	($f_c = 20$)	0.1913	186.0000	333.8027	0.1694	0.9439	22.8959	1.0738
Gaussian	($f_c = 30$)	0.0822	170.0000	253.3742	0.1473	0.9564	24.0931	1.0570
Optimum Value		**−0.2327**	**42.0000**	**46.3289**	**0.0588**	**0.9152**	**31.4722**	1.**0198**

$$\mu_{c_1}(t) = \sum_{j=1}^{t} \frac{j\mathrm{P}(j)}{K_1(t)} \mu_{c_2}(t) = \sum_{j=t+1}^{S} \frac{j\mathrm{P}(j)}{K_2(t)} \tag{15}$$

Table 3 Performance metrics of different denoising filters for test image 3

Filters	Window Size/Frequency	Performance Metrics						
		AD	MD	MSE	NAE	NK	PSNR	SC
Frost	3 × 3	0.0276	55.0000	**37.0888**	**0.0521**	0.9912	**32.4383**	**1.0138**
Frost	5 × 5	0.0541	70.0000	107.5218	0.0902	0.9823	27.8158	1.0250
Frost	7 × 7	0.0843	75.0000	164.0150	0.1113	0.9756	25.9819	1.0331
Lee	3 × 3	−0.0002	82.0000	214.1841	0.1252	0.9739	24.8229	1.0317
Lee	5 × 5	0.0010	97.0000	308.4888	0.1504	0.9631	23.2384	1.0449
Lee	7 × 7	0.0043	112.0000	381.5348	0.1672	0.9552	22.3154	1.0544
Kuan	3 × 3	0.4110	176.0000	253.9536	0.1305	0.9685	24.0832	1.0391
Kuan	5 × 5	0.4032	188.0000	274.0230	0.1598	0.9756	23.0082	1.0432
Kuan	7 × 7	0.4124	201.0000	284.0345	0.1675	0.9832	22.2378	1.0501
Median	3 × 3	1.9257	168.0000	317.5381	0.1457	0.9457	23.1128	1.0835
Median	5 × 5	1.9257	168.0000	317.5381	0.1457	0.9457	23.1128	1.0835
Median	7 × 7	1.9257	168.0000	317.5381	0.1457	0.9457	23.1128	1.0835
Wiener	3 × 3	**−0.0180**	**45.0000**	121.2349	0.0979	0.9826	27.2945	1.0232
Wiener	5 × 5	0.0209	62.0000	182.7343	0.1202	0.9744	25.5126	1.0342
Wiener	7 × 7	0.1128	71.0000	231.1678	0.1350	0.9675	24.4915	1.0438
Gaussian	($f_c = 10$)	0.8606	141.0000	527.6828	0.1965	**0.9265**	20.9070	1.1044
Gaussian	($f_c = 20$)	0.2174	111.0000	356.6203	0.1613	0.9530	22.6087	1.0622
Gaussian	($f_c = 30$)	0.0996	95.0000	267.2149	0.1397	0.9641	23.8622	1.0474
Optimum Value		**−0.0180**	**45.0000**	**37.0888**	**0.0521**	**0.9265**	**32.4383**	**1.0138**

where S is the no of gray level. The optimal threshold t^* is as follows

$$t^* = \arg\min_t \sigma_w^2(t) \tag{16}$$

Where σ_w^2 is the within class variance

$$\sigma_w^2(t) = K_1(t)\sigma_1^2(t) + K_2(t)\sigma_2^2(t) \tag{17}$$

Where K_1, K_2, σ_1^2, $\sigma_2^2$are the estimated group probabilities and group variances. They are calculated as

$$K_1 = \sum_{j=1}^{t} \mathrm{P}(j) \quad K_2 = \sum_{j=t+1}^{S} \mathrm{P}(j) \tag{18}$$

$$\sigma_1^2(t) = \sum_{j=1}^{t} \left[i - \mu_{c_1}(t)\right]^2 \frac{\mathrm{P}(j)}{K_1(t)} \sigma_2^2(t) = \sum_{j=t+1}^{S} \left[j - \mu_{c_2}(t)\right]^2 \frac{\mathrm{P}(j)}{K_2(t)} \tag{19}$$

where the gray level range varies from 1 to S. The result of the Otsu method is shown in Fig. 10. The Otsu's method does not produce satisfactory result to extract follicles from ovary image. The performance of the Otsu method leads to do modification in it to obtain accurate results.

4.2 Proposed method

The proposed method provides an automatic method for follicle extraction from ultrasound ovary images using active contour without edges method [7]. In region based active contour initial contour can be placed anywhere in the image. The contour initialization is the difficult task, the poor initialization can produce the contour away from the follicles region. In order to automate the segmentation process, the ovary image is binarized using modified Otsu method and the resultant image is used as a binary mask for initialization of the level set method. The

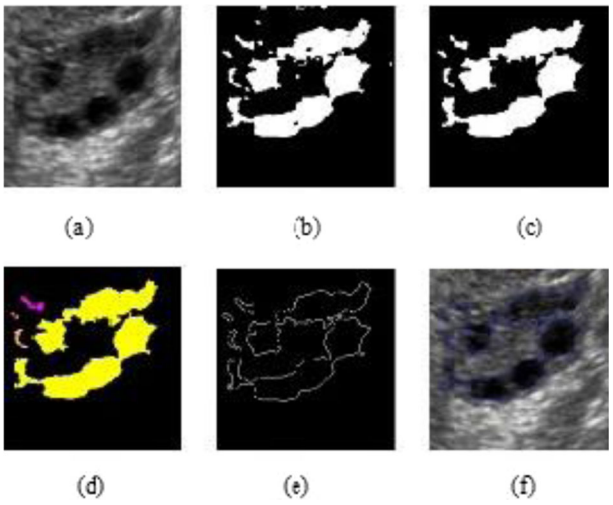

Fig. 10 (a) A ultrasound ovary image with follicles.(b) The result given by the conventional Otsu's method. (c) Area open image. (d) The result of the counted follicles. (e) The result of the edge detected image. (f) Superimposed on original Image

binary mask contains only two regions background and foreground which is as close as to the segmented object it can solve the problem of contour initialization. The proposed segmentation method begins with thresholding the ovary image using Modified Otsu method. In thresholding technique the objects are extracted from the image based on distribution of gray levels. The traditional Otsu method fails to segment the follicles accurately which is shown in Fig. 10. From the result we understand that Otsu method produces correct result only when the image histogram is bimodal. The proposed modified Otsu method produces accurate results for all types of histogram.

4.3 Modified Otsu method

The thought of estimating initial threshold value in Otsu method using iterative method is introduced here. Initially the threshold T_1 is the average value of the ovary image. At the first iteration, the intensity of the image which is greater than or equal to the threshold T_1 is identified. In the next step, mean value above current threshold and mean value below current threshold are calculated which is denoted as $m_1^{[31]}$, $m_2^{[1]}$.

The new set of threshold is calculated as

$$T[1] = \frac{m_1^{[1]} + m_2^{[1]}}{2} \tag{20}$$

The newly calculated threshold value *T[1]* carry forward to the next iteration. The superscript denotes the number of iterations. At the second iteration, the intensity of the image which is greater than or equal to the current threshold *T[1]* is find. In the second iteration the mean value $m_1^{[2]}$ below the current threshold *T[1]* and mean value $m_2^{[2]}$ above *T[1]* is calculated. Similarly, the second iteration calculates the threshold value

$$T[2] = \frac{m_1^{[2]} + m_2^{[2]}}{2} \tag{21}$$

The iteration stops until the threshold value converges$T[K] - T[K-1]$. At the last iteration the new threshold value is calculated as

$$t^{**} = \frac{m_1{}^{[K]} + m_2{}^{[K]}}{2} \tag{22}$$

The between class variance of the conventional Otsu method was defined as

$$\sigma_B^2(t) = K_1\left(\mu_{c_1} - \mu_t\right)^2 + K_2\left(\mu_{c_2} - \mu_t\right)^2 \tag{23}$$

Now, iteratively calculated threshold value t^{**} in Eq. (22) is used as an initial threshold for conventional Otsu method.

Where μ_{c_1}, μ_{c_2} are means of two groups

$$\mu_{c_1}(t) = \sum_{j=1}^{t^{**}} \frac{j\mathrm{P}(j)}{K_1(t)\mu_{c_1}(t)} \tag{24}$$

$$\mu_{c_2}(t) = \sum_{j=t^{**}+1}^{S} \frac{j\mathrm{P}(j)}{K_2(t)} \tag{25}$$

The total mean μ_t the whole image is given in the Eq. (26)

$$\mu_t = \sum_{j=1}^{S} j\Pr(j) \tag{26}$$

4.3.1 Initialization of mask

The modified Otsu method produces the binary image consists only background (zero) and object (white), in the proposed method which is used as a binary mask in order to initialize the contour position. For accurate and faster diagnosis, specifying initial contour position which is closest to the preferred object boundaries is needed. The initial mask for the level set algorithm is shown in Fig. 11(e). The level set method was proposed by Osher and Sethian [32]. In the implementation of active contour with level set method provide flexibility. The interface C is internally denoted as function ϕ for a level set function. This is rather represented as scalar function$C = \{(y, z), \phi(y, z) = 0\}$.

The Signed Distance function is obtained from initial mask. The narrow band approach is used to reduce the computation time taken by level set method to make a ϕ change [32]. The values of the ϕ are updated which is exist within the narrow band. The curves narrow band is given by the equation

$$C_{nb} = \{(i, j) - \beta \leq \beta, i = [0, n-1], j = [0, m-1]\} \tag{27}$$

The mean curvature of the level set function is given by

$$curvature = \frac{\left(\phi_y^2 * \phi_{zz} + \phi_z^2 * \phi_{yy} - 2\phi_y \phi_z \phi_{yz}\right)}{\left(\phi_y^2 + \phi_z^2\right)^{\frac{3}{2}}} \tag{28}$$

where $\phi_y$and ϕ_{yy}denote the first and second-order partial derivatives of ϕ with respect to y, and $\phi_z$and ϕ_{zz}denote the same with respect to z which is given by

$$\phi_y^2 = \left(\frac{\partial \phi}{\partial y}\right)^2 \phi_z^2 = \left(\frac{\partial \phi}{\partial z}\right)^2 \phi_{yy} = \left(\frac{\partial^2 \phi}{\partial y^2}\right) \phi_{zz} = \left(\frac{\partial^2 \phi}{\partial z^2}\right) \phi_{yz} = \left(\frac{\partial^2 \phi}{\partial yz}\right)$$

The Central difference approximation is given by

$$\begin{aligned} \phi_y &= -\phi(P_l) + \phi(P_r) \\ \phi_z &= -\phi(P_d) + \phi(P_u) \\ \phi_{yy} &= -\phi(P_l) - 2\phi(P) + \phi(P_r) \\ \phi_{zz} &= -\phi(P_d) - 2\phi(P) + \phi(P_u) \end{aligned} \tag{29}$$

Each of the derivatives of ϕ is estimated in relation to y and z. The value of ϕ after a small time interval Δt was approximated by the first-order Taylor expansion given by equation$\phi_t$is defined by gradient descent and Δt is the time step.

$$\begin{aligned} \phi((y, z), t + \Delta t) &= \Delta t * \phi_t + \phi((y, z), t) \\ \phi_t &= \alpha * curvature + \frac{F}{\max|F|} \\ \Delta t &= \frac{1}{(\max(\phi_t) + \varepsilon)} \end{aligned} \tag{30}$$

where α is the weight of a smoothing term and ε is coefficient to satisfy Courant, Friedrichs, Lewy (CFL) condition [28]. Whereas resolve certain partial differential equations CFL condition is essential.

Fig. 11 Axis of ellipse

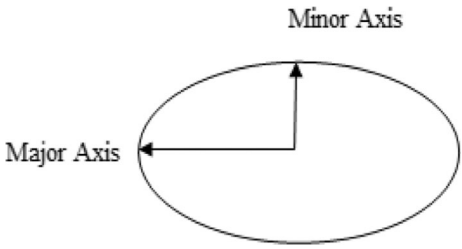

The Sussman function [8] is used to smooth the SDF

$$\phi_{i,j}^{M+1} = \phi_{i,j}^{M} - \Delta t S_{\varepsilon}(\phi_{i,j}) G\left(\phi_{i,j}^{M}\right) \tag{31}$$

Where,

$$S_{\varepsilon}(\phi)_{i,j} = \frac{\phi_{i,j}^2}{\sqrt{\left(\phi_{i,j}^2 + \varepsilon^2\right)}}$$

$$H\left(\phi_{i,j}^{N}\right) = \begin{cases} \sqrt{\left(\max(K^+)^2, (L^-)^2 + \max\left((M^+)^2, (N^-)^2\right)\right)} - 1 \\ \sqrt{\left(\max(K^-)^2, (L^+)^2 + \max\left((M^-)^2, (N^+)^2\right)\right)} - 1 \\ 0 \, otherwise \end{cases}$$

The combination of modified Otsu with active contour provides better segmentation results. From the segmented results necessary information are extracted for further diagnosis.

Table 4 Feature extraction from Otsu's results

Method	Individual Follicle	Area	Perimeter	Major Axis	Minor Axis	Eccentricity
Otsu	1	1403	146.2254	47.7929	38.8989	0.5809
	2	830	122.9117	39.7743	29.5237	0.6700
	3	394	77.5979	26.4367	19.5553	0.6729
	4	495	101.3970	42.1903	15.7462	0.9277
	5	857	114.5685	35.5344	31.6657	0.4537
	6	74	35.3137	14.7099	6.9835	0.8801
	7	671	101.4975	33.1268	26.5182	0.5993
	8	689	103.4975	31.5136	28.6852	0.4140
	9	96	48.7279	20.8672	7.09851	0.9403
	10	135	60.5269	25.5746	8.1232	0.9482
	11	3741	417.7473	103.0747	61.3126	0.8038
	12	1608	174.9949	49.3048	44.2275	0.4419
	13	195	57.4558	20.1046	13.0143	0.7622
	14	103	44.3847	18.2615	8.19804	0.8935
	15	1901	176.0244	58.2410	42.3615	0.6862
	16	83	41.5563	16.5129	7.2268	0.8991
	17	528	191.8234	53.1546	26.2380	0.8696
	No of Follicles Identified: 17					

5 Extraction of features

The objective of the feature extraction technique is to extract typical information which is useful for diagnosis and classification of diseases. The shape based features Area, Perimeter, Eccentricity, Majoraxis, Minoraxis are extracted from ultrasound ovary images. The size and number for the follicle is used for classifying the image as cystic ovary, normal ovary, and polycystic ovary. The shape based information is extracted from segmented results obtained from different methods those are listed in the Tables 4, 5 and 6.

5.1 Area

Area of an object in the image is generally defined as the number of pixels inside the object. Thereby, the area of a follicle in an ovary imageis determined by the number of pixels constituting the follicle. It is used to identify the size of the follicle.

5.2 Perimeter

The perimeter is the overall length of the object boundary which is calculated by the distance among each neighboring pair of pixels around the edge of the region.

5.3 Eccentricity

The ratio of the distance between the region of the follicle and its major axis length is known as Eccentricity.

5.4 Majoraxis&Minoraxis

The diameter is the minor as well as major axes of an ellipse. The major axes includes longest diameter of an ellipse and minor-axes includes the shortest diameter of an ellipse.

Table 5 Feature extraction from modified Otsu's results

Method	Individual Follicle	Area	Perimeter	Major Axis	Minor Axis	Eccentricity
Modified Otsu	1	1269	139.8823	45.0114	37.5171	0.5525
	2	311	68.5269	23.3240	17.6308	0.6546
	3	732	112.0833	37.8439	27.0226	0.7000
	4	412	96.5685	39.6104	13.9217	0.9362
	5	761	106.6690	32.5269	30.5955	0.3394
	6	580	98.0832	30.9033	24.6577	0.6027
	7	589	92.4264	29.5845	26.0111	0.4764
	8	1767	255.0366	70.9228	34.6200	0.8727
	9	1417	150.7107	47.0169	39.9255	0.5281
	10	1000	189.4386	44.7331	33.0268	0.6744
	11	1759	171.6812	55.8660	40.9404	0.6804
	12	52	27.8994	9.7820	7.6236	0.6265
	No of Follicles Identified: 12					

Table 6 Feature extraction from proposed method results

Method	Individual Follicle	Area	Perimeter	Major Axis	Minor Axis	Eccentricity
Proposed Method	1	316	66.2842	22.5176	18.5406	0.5674
	2	74	29.8994	11.4336	8.4547	0.6731
	3	176	51.2132	18.2017	13.3194	0.6815
	4	97	40.6274	18.3712	6.9437	0.9258
	5	185	49.2132	15.9711	15.0886	0.3278
	6	142	44.6274	15.1518	12.2587	0.5877
	7	143	42.9705	14.6643	12.7131	0.4983
	8	435	104.0833	34.9467	17.0111	0.8735
	9	353	70.2842	23.3807	19.8720	0.5268
	10	242	74.8700	21.7270	15.8405	0.6844
	11	436	79.1127	27.8337	20.2830	0.6848
	No of Follicles Identified: 11					

6 Experimental results

The proposed method has been validated by applying it to a various ultrasound ovary images. For this study, the ultrasound images of ovaries are collected from Nandhini Sri Diagnostic Center after consultation with Radiologist and Gynecologist. The images are captured by the GE LOGIQ ultrasound system which is having 24 Hz transvaginal transducer frequency. The simulation is processed using the 65 sample ultrasound-images of ovaries. The experiments have been executed on Hp Pavilion dv5 with Intel® Core™ 2 Duo CPU @ 2.00GHz with 3 GB of RAM running on Microsoft Windows 7 platform. The proposed method is implemented using Matlab programming language on the Matlab 2012a software.

The Fig. 10 (a) shows an original ultrasound ovary image and Fig. 10(b) presents the result given by the conventional Otsu's method. Many undesired regions are also found in the segmented result it is necessary to remove these undesired regions. Hence the objects having area less than 50 are removed and the objects touching the border also removed from Fig. 10(b) which is shown in Fig. 10(c). From the segmented results the size and the number of follicles are extracted for diagnosis. The number of identified follicles is shown in Fig. 10(d). Based on the number of follicles and its size the ultrasound ovary images are classified into cyst, PCOS and normal ovary, accurate detection of follicles results in correct diagnosis. The Fig. 10(e) represents the detected edges of the follicles and the Fig. 10 (f) shows the segmented follicles superimposed on the original image.

Fig. 12(a) represents the original image and the Fig. 12(b) shows the histogram of an original image. The input images are preprocessed for better diagnosis based on the optimum value obtained from Tables 1, 2 and 3 the filter is chosen to denoised the original image. The Frost filtered image is shown in Fig. 12(c). As can be seen from the experimental results we come to know all follicles are not correctly identified by the Otsu method. The modified Otsu method binarizes the image the result is shown in the Fig. 12(d). The objects touching the border removed also the objects with less than 50 pixels are removed. The Fig. 12(e) illustrates the binary mask obtained from modified Otsu method which is further used as an initializing mask in proposed method. The proposed method exactly segment all follicles present in the image which is illustrated in the Fig. 12(f). The number of follicles and its size is used to classify the image. Therefore, the number of follicles is counted which is shown in the Fig. 12(g) and its shape information extracted. The edges of the objects are detected from the Fig. 12(f). Then using this information the extracted follicles are superimposed on original

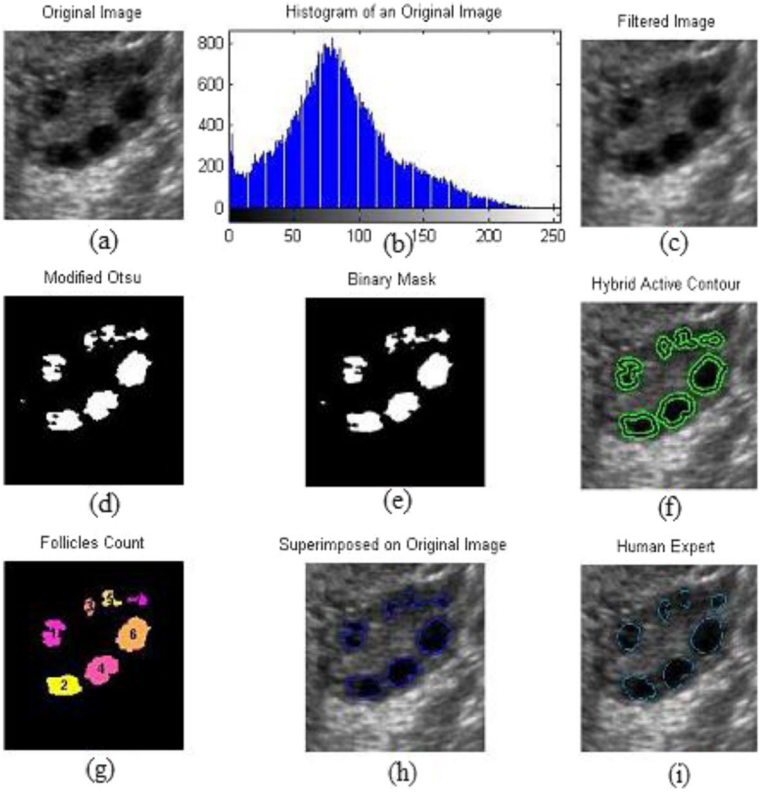

Fig. 12 (a) Ovary Image.(b) Histogram of an Ovary Image. (c) The result given by Frost filter. (d) The result given by Modified Otsu. (e) Mask initialization. (f) The result given by proposed method. (g) The result of the identified follicles. (h) The result superimposed on original image (i) Manual detection by medical expert

image as depicted in Fig. 12(h). The Fig. 12(i) shows the detection of manual follicle that is done by the medical expert. Manual follicle detection done by the medical expert. This automatic method demonstrates the efficiency of the proposed technique.

The Fig. 13 sample shows the resultant image owing to the fact that the proposed method produces better among all the other methods. The shape feature information is extracted from the segmented results yielded by different segmentation methods. The Fig. 14 shows the number of follicles identified by proposed method in comparison to the previously mentioned segmentation methods for three ultrasound ovary images. For Test Image 1 Otsu method detects 4 follicles and modified Otsu method detects 6 follicles finally the proposed method exactly detects 7 follicles. The automatic detection method classifies Test Image 1 as normal ovary, Test Image 2 as Cystic Ovary and the Test Image 3 is classified as Polycystic Ovary. The shape features are extracted from the segmented image yield by Otsu method, modified Otsu method, and the proposed method. The shape information Area, Perimeter, Majoraxis, Minoraxis and Eccentricity are calculated which is shown in the Tables 4, 5, 6. As can be seen from the results the proposed method yields more accurate results than other methods also the obtained results equivalent the manual detected results by the medical expert. Based on the experimental results obvious improvements can be seen in the proposed algorithm, furthermore it achieves accurate automatic diagnosis of PCOS on ultrasound ovary images.

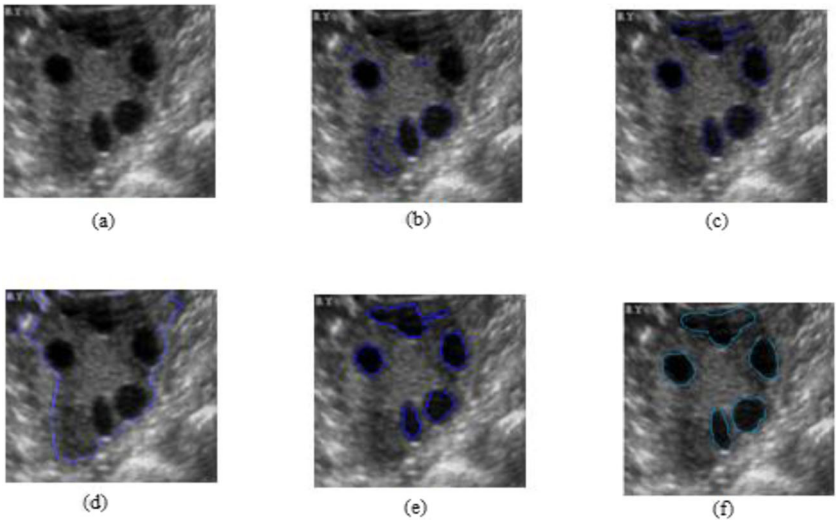

Fig. 13 Some distinctive results for 3 input images a) Original Image b) Segmentation by Otsu method c) Segmentation by Modified Otsu d) Segmentation by Active Contour e) Segmentation by Proposed method

7 Conclusion and future work

This work presents a computationally efficient method for automatic follicle detection and segmentation of ovarian follicles from the ultrasound ovary image. In this paper the result of the modified Otsu method is taken as an initial mask for the level set formulation. Compared

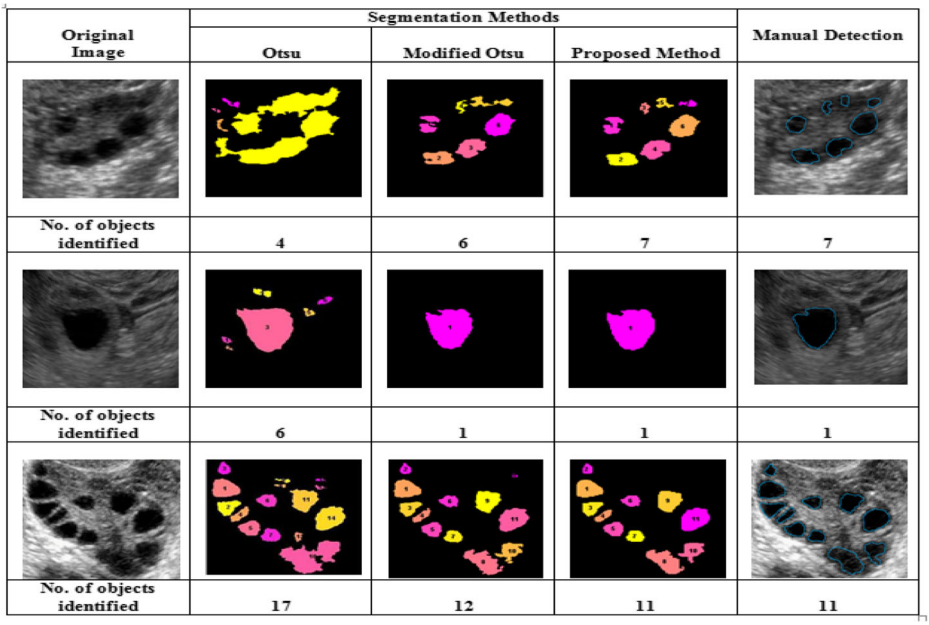

Fig. 14 Difference in follicle counts identified by the Otsu method, by the modified Otsu method by the proposed method and by the experienced medical expert for three different ultrasound ovary images

with Otsu method the modified Otsu method provides the more accurate segmented results. The combination of modified Otsu method with active contour detects the exact number of follicles from the ultrasound ovary image. The proposed method outperforms than the other known techniques based in terms of accuracy. Hence these proposed methods are well suited for extraction of follicles from the ovary images. The medical expert study the women's menstrual cycle and assesses the follicles inside the ovaries of woman who undergoes infertility treatment for this automatic diagnostic system is needed to reduce the computational complexity. The automatic diagnostic method reduces the trouble of the radiologist and Gynecologists without give up the accuracy of diagnosis. This work will be look forward to helpful in the development of software tool embedded in the ultrasound system. In future the segmented images are classified using best classification method with large database.

References

1. Abdel-Basset M, Manogaran G, Fakhry AE, El-Henawy I (2018) 2-levels of clustering strategy to detect and locate copy-move forgery in digital images. Multimed Tools Appl, 1–19
2. Adam B, Joop SE, Laven S-LT, Dewailly D (2003) Ultrasound assessment of the polycystic ovary: international consensus definitions. Hum Reprod 9(6):505–514
3. Affiliates of Medifocus.com (2007) Medifocus guidebook: polycystic ovary syndrome. Medifocus.com, Inc
4. Bal and H. Mohan (2007) Malignant transformation in mature cystic Teratoma of the ovary: report of five cases and review of the literature. Arch Gynecol Obstet 275(3):179–182
5. Battaglia C, Artini PG, Genazzani AD, Gremigni R, Slavatori MR, Sgherzi MR (1997) Color Doppler analysis in oligo and Amenorrheic women with polycystic ovary syndrome. Gynecol Endocrinol 11(2): 105–110
6. Caselles V, Kimmel R, Sapiro G (1997) On geodesic active contours. Int J Comput Vis 22(1):61–79
7. Chan T, Vese L (2001) Active contours without edges. IEEE Trans Image Process 10(2):266–277
8. Courant R, Friedrichs K, Lewy H (1928) Uber die partiellenDifferenzengleichungen der mathematischenPhysik. MathematischeAnnalen 100(1):32–74. http://en.wikipedia.org/wiki/Courant%E2%80%93Friedrichs%E2%80%93Lewy_condition
9. Deng Y, Wang Y, Chen P (2008) Automated detection of polycystic ovary syndrome from ultrasound image. 30th annual international IEEE engineering in medicine and biology society conference Vancouver, British Columbia, Canada: 20-24
10. Deng Y, Wang Y, Shen Y (2011) An automated diagnostic system of polycystic ovary syndrome based on object growing. J Artif Intell Med Elsevier Sci Publishers Ltd Essex, UK 51(3):199–209
11. Finn S, Glavin M, Jones E (2011) Echocardiographic speckle reduction comparision. IEEE Trans Ultrason Ferroelectr Freq Contrl 58(1):82–101
12. Frost VS, Stiles JA, Shanmugam KS, Holtzman JC (1982) A model for radar image & its application to adaptive digital filtering for multiplicative noise. IEEE Trans Pattern Anal Mach Intell PAMI-4(2):157–166
13. Gharbia R, Hassanien AE, El-Baz AH, Elhoseny M, Gunasekaran M (2018) Multi-spectral and panchromatic image fusion approach using stationary wavelet transform and swarm flower pollination optimization for remote sensing applications. Futur Gener Comput Syst 88:501–511
14. Gonzalez RC, Woods RE (2002) Digital image processing, Second Edition, Pearson Edu
15. Hanna MD, Chizen DR, Pierson R (1994) Characteristics of follicular evacuation during human ovulation. J Ultrasound Obstetr Gynecol 4(6):488–493
16. Hiremath PS, Jyothi Tegnoor R (2011) Automatic detection of follicles in ultrasound images of ovaries using active contours method. Int J Serv Comput Comput Intell 1(1):26–30
17. Hiremath PS, Tegnoor JR (2010) Automatic detection of follicles in ultrasound images of ovaries using edge based method. International Journal of Computer Applications Special Issue on Recent Trends in Image Processing and Pattern Recognition: 15–16
18. Iyapparaja M, Sivakumar P (2017) Metrics based evaluation for disease affection in distinct cities. Res J Pharm Tech 10(8):2487–2491
19. Iyapparaja M, Tiwari M (2017) Security policy speculation of user uploaded images on content sharing sites. IOP Conf Ser: Mater Sci Eng 263:042018. https://doi.org/10.1088/1757-899X/263/4/042019 pp-1-8
20. Kelsey TW, Wallace WHB (2012) Ovarian volume correlates strongly with number of non growing follicles in the human ovary. Obstet Gynecol Int 2012:1–5

21. Kuan DT, Sawchuk AA, Strand TC, Chavel P (1985) Adaptive noise smoothing filter for images with signal-dependent noise. IEEE Trans Pattern Anal Mach Intell PAMI-7(2):165–177
22. Lee JS (1980) Digital image enhancement and noise filtering by using local statistics. IEEE Trans Pattern Anal Mach Intell PAMI-2(2):165–168
23. Mehrotra P, Chakraborty C (2011) Automated ovarian follicle recognition for polycystic ovary syndrome. International Conference on Image Information Processing: 1–4.
24. Michailovich OV, Tannenbaum A (2006) Despeckling of medical ultrasound images. IEEE Trans Ultrason Ferroelectr Freq Control 53(1):64–78
25. Murugan NS, Devi GU (2018) Cluster Comput. doi:https://doi.org/10.1007/s10586-018-2158-3
26. Murugan NS, Usha Devi G (2018) Detecting streaming of twitter spam using hybrid method. Wirel Pers Commun : 1-22
27. Nicolae MC (2010) Comparative approach for speckle reduction in medical ultrasound images. Romanian J Bio-Phys 20(1):13–21
28. Osher S, Sethian JA (1988) Fronts propagating with curvature-dependent speed: algorithms based on Hamilton-Jacobi formulation. J Comput Phys 79:12–49
29. Otsu N (1979) A threshold selection method from gray-level histograms. IEEE Trans Syst Man Cybernet 9(1):62–66
30. Pache TD, WWladimiroff J, Hop WC, CFauser B (1992) How to discriminate between Normal and polycystic ovaries: transvaginal US study. Radiology 183(2):421–423
31. Pellicer A, Gaitán P, Neuspiller F, Ardiles G, Albert C, Remohí J, Simón C (1998) Ovarian follicular dynamics: from basic science to clinical practice. J Reprod Immunol 39(1-2):29–61
32. Phillips C (1999) The level-set method. MIT Undergraduate Journal of Mathematics
33. Ratha TJ, Ramar K (2010) A modified method for speckle noise removal in ultrasound medical images. Int J Comput Electric Eng 2(1):54–58
34. Sudha S, Suresh GR, Sukanesh R (2009) Speckle noise reduction in ultrasound images by wavelet thresholding based on weighted variance. Int J Comput Theor Eng 1(1):7–12
35. Yamanaka Y, Tateiwa Y (2005) Preoperative diagnosis of malignant transformation in mature cystic Teratoma of the ovary. Eur J Gynecologic Oncol 26(4):391–392

C. Gopalakrishnan received his Bachelor's in Information Technology (with first class) from Anna University, Chennai, Tamilnadu, India in 2012 and Master's in Information Technology (with first class) from VIT University, Vellore, Tamilnadu, India in 2015, and currently working towards his PhD in Information Technology in VIT University, Vellore, Tamilnadu, India. His research interests include Big Data and Image Processing.

Iyapparaja Meenakshisundaram , He received Ph. D in Anna University, Chennai, BE degree from Anna University, Chennai and ME degree from Anna University of Technology, Coimbatore. Presently, He is an Associate Professor in School of Information Technology and Engineering, VIT, Vellore. He has 11 years of experience in Teaching and Big data, Software testing and software Engineering field. He received University Rank holder award for his ME degree. His research interests include Software Testing, Software Engineering, Big data, Networking and Agile Testing. He is life time member of ISTE.